Deep Multi-Sensor Domain Adaptation on Active and Passive Satellite Remote Sensing Data

Xin Huang
Department of Information Systems, University of Maryland, Baltimore County
Baltimore, MD, USA
xinh1@umbc.edu

Sahara Ali
Department of Information Systems, University of Maryland, Baltimore County
Baltimore, MD, USA
sali9@umbc.edu

Sanjay Purushotham
Department of Information Systems, University of Maryland, Baltimore County
Baltimore, MD, USA
psanjay@umbc.edu

Jianwu Wang
Department of Information Systems, University of Maryland, Baltimore County
Baltimore, MD, USA
jianwu@umbc.edu

Chenxi Wang
Goddard Space Flight Center, National Aeronautics and Space Administration
Greenbelt, MD, USA
chenxi.wang@nasa.gov

Zhibo Zhang
Department of Physics, University of Maryland, Baltimore County
Baltimore, MD, USA
zhibo.zhang@umbc.edu

ABSTRACT

Studies have shown machine learning (ML) algorithms such as Random Forests (RF) could outperform the physical-based algorithms in remote sensing applications. However, these ML algorithms are not well-suited to learn from heterogeneous sources such as multiple active and passive sensors. For example, RF can be either developed for Cloud-Aerosol Lidar and Infrared Pathfinder Satellite Observations (CALIPSO) or Visible Infrared Imaging Radiometer Suite (VIIRS) sensor data, but it cannot jointly learn from both these sensors since there is a mismatch of features (variables) among the sensors. On the other hand, domain adaptation techniques have been developed to handle data from multiple sources or domains. But most existing domain adaptation approaches assume that the source and target domains are homogeneous i.e., they have the same feature space, and the difference between domains primarily arises due to the data distribution drifting. Nevertheless, many real world applications often deal with data from heterogeneous domains that come from completely different feature spaces. For example, in our remote sensing application, the source domain, namely CALIPSO, contains data of 25 attributes collected by the active spaceborne Lidar sensor; and the target domain, namely VIIRS, contains another group of data of 20 attributes collected by passive spectroradiometer sensor. CALIPSO has better representation capability and sensitivity to aerosol types and cloud phase, while VIIRS has wide swaths and better spatial coverage but has inherent weakness in differentiating atmospheric objects on different vertical levels. To address this mismatch of features across the domains (sensors), we propose a novel deep learning based heterogeneous domain adaptation framework called Deep Multi-Sensor Domain Adaptation (DMSDA) to 1) learn the domain invariant representations from source CALIPSO and target VIIRS domains by transferring the knowledge across these domains, and 2) better classify the different cloud phase types in the source and target domains. Our experiments on a collocated CALIPSO and VIIRS sensor dataset showed that DMSDA can achieve 69% classification accuracy in predicting the cloud phase types that is at least 23% improvement and outperformed other ML approaches employed in comparison.

KEYWORDS

domain adaptation, remote sensing, cloud type detection, deep learning, machine learning

ACM Reference Format:
Xin Huang, Sahara Ali, Sanjay Purushotham, Jianwu Wang, Chenxi Wang, and Zhibo Zhang. 2020. Deep Multi-Sensor Domain Adaptation on Active and Passive Satellite Remote Sensing Data. In *DeepSpatial 2020, August 24, 2020, SIGKDD Workshop*. ACM, New York, NY, USA, 9 pages. https://doi.org/10.1145/1122445.1122456

1 INTRODUCTION

Cloud and atmospheric aerosols are two critical components that significantly impact Earth's radiative energy balance, hydrological and biological cycles, air quality and human health [4]. For example, clouds constantly cover about two-third of Earth's surface and alter global energy distribution by reflecting solar radiation and absorbing thermal emission from the surface. Satellite-based remote sensing is the only means to monitor the global distribution of aerosols and clouds. Thus, improvements in aerosol and cloud observations are a major focus of NASA's Earth Science endeavor, and numerous satellite sensors have been developed to observe and retrieve aerosol and cloud properties. They can be largely divided into two groups: active sensors such as spaceborne Lidar (e.g., CALIPSO) and Radar (e.g., CloudSat) and passive sensors such as Moderate Resolution Imaging Spectroradiometer (MODIS), VIIRS

DeepSpatial '20, August 24, 2020, KDD Virtual Conference

ACM ISBN 978-x-xxxx-xxxx-x/YY/MM…$15.00
https://doi.org/10.1145/1122445.1122456

and Advanced Baseline Imager (ABI). Active sensors collect data by providing their own source of energy to illuminate the objects they observe; while passive sensors collect different sets of data attributes by detecting natural energy (radiation) that is emitted or reflected by the object. The advantages of active sensors, compared to passive sensors, include their capability of resolving the vertical location of aerosol/cloud layer; better sensitivity to aerosol type and cloud phase; better performance during nighttime and polar region. On the other hand, passive sensors have sensors that observe column integrated radiation and have inherent weaknesses in differentiating atmospheric objects on different vertical levels. However, passive sensors always have wide swaths and better spatial coverage. Classifying the pixel level cloud types is an important application in the satellite remote sensing. By employing both active and passive sensing data, we aim to classify 6 cloud types, which are Clear and Clean (no cloud, no aerosol), Pure Liquid Cloud (no ice cloud, no aerosol), Pure Ice Cloud (no liquid cloud, no aerosol), Pure Cloud (have both ice and liquid clouds, no aerosol), Pure Aerosol (no cloud, aerosol only), Cloud and Aerosol.

Our previous study [21] has shown proper use of machine learning algorithms, such as Random Forest (RF), can have better cloud type detection accuracy than physical-based algorithms. However, the algorithms cannot directly learn from multiple active and passive sensors. For example, RF can be either developed for CALIPSO or VIIRS data, but it cannot jointly learn from both these sensors since there is a mismatch of features (variables) among the sensors. RF and other ML algorithms do not generalize to new combinations of the learned features beyond those seen during the training process. Moreover, many ML algorithms generally cannot do joint label predictions if the labels are missing for one of these sensors during training time. To address these issues, we employ deep learning (DL) models which can automatically learn feature representations from multiple sensors with different features / variables in an end-to-end fashion. Our DL models will be able to predict labels for all sensors even when the labels are absent for some sensors at training time by transferring knowledge from one set of sensors (e.g., CALIPSO) to other sensors (e.g., VIIRS).

Domain adaptation has been thoroughly studied in computer vision [7] , [5] and natural language processing (NLP) applications [3], [6]. Recently, the deep learning paradigm has become popular in domain adaptation due to its ability to learn rich, flexible, non-linear domain-invariant representations [18], [16]. However, few of these approaches have been adapted for remote sensing applications. Moreover, domain adaptation techniques using deep neural network have been mainly used to solve the distribution drifting problem in homogeneous domains [17]. The data in the homogeneous domains usually share similar feature spaces and have the same dimensionalities. Nevertheless, real world applications often deal with heterogeneous domains that come from completely different feature spaces and different dimensionalities. In our remote sensing application, the two remote sensor datasets collected by active and passive sensors respectively are heterogeneous. In particular, CALIPSO actively collects 25 bands of sensing data, it has better sensitivity to aerosol types and cloud phase, and the data are fully labeled with 6 cloud types. VIIRS uses spectroradiometer sensor to passively collect 20 bands of sensing data with no label for cloud types; has wide swaths and better spatial coverage but lacks the sensitivity to the cloud types.

Our contribution is to classify different cloud types for the massive unlabeled records in the passive / target domain data (VIIRS) by learning the transferable representation of the cloud types from the active source domain (CALIPSO). We develop an unsupervised Deep Multi-Sensor Domain Adaptation (DMSDA) model to learn feature representations from multiple heterogeneous sensors. Our experiments show the effectiveness of our approach in learning the domain invariant representation for the heterogeneous domains.

2 RELATED WORK

Over the past few decades, a variety of aerosol and cloud remote sensing algorithms have been developed based on the physical principles and the radiative transfer of light scattering and absorption within aerosol and cloud fields (see review by [2]). These physical-based algorithms are the backbone of many widely used aerosol and cloud property products for weather and climate studies [1],[10]. Traditionally, many of these algorithms use a lookup table (LUT) approach, in that one must prescribe aerosol and surface properties. The challenge is to ensure that the algorithm has the means to select the appropriate model.

Although highly successful, it is challenging to improve these physical-based algorithms. For example, according to [14], there is no absolute separation between "aerosol" and "cloud". Most, if not all, retrieval techniques that rely on manually setting thresholds for scene calibration, etc., may be different enough that a threshold applied for one sensor may need revision for another. Thus, physical-based algorithms are expensive.

Machine Learning (ML) and Artificial Intelligence (AI) techniques may overcome the challenges facing physical-based algorithms. Since ML algorithms are written to autonomously find information (e.g., patterns of spectral, spatial, and/or time series), they can learn hidden signatures of different types of objects. ML algorithms are portable and can be easily applied to active and/or passive sensor measurements. [21] introduced two Random Forest (RF) machine learning models for cloud mask and cloud thermodynamic phase detection using spectral observations from Visible Infrared Imaging Radiometer Suite (VIIRS) on board Suomi National Polar-orbiting Partnership (SNPP). [24] developed a deterministic self-organizing map (SOM) approach and applied it on satellite data based cloud type classification. Deep learning [11] is also a promising technique, already having revolutionized many fields such as computer vision [8], natural language processing [15], and is increasingly being used in remote sensing applications [23]. Those approaches can learn representations of multiple variables in a single domain.

Domain Adaptation has been widely used in learning domain invariant representation from source and target domains. In unsupervised domain adaptation with unlabeled target domain, Several approaches have been developed to minimize the feature distribution difference between the source domain and target domain. DCC [20] and DAN [13] have used Maximum Mean Discrepancy (MMD) loss training the deep neural network and learn a representation that is both discriminative and domain invariant. [17] introduced

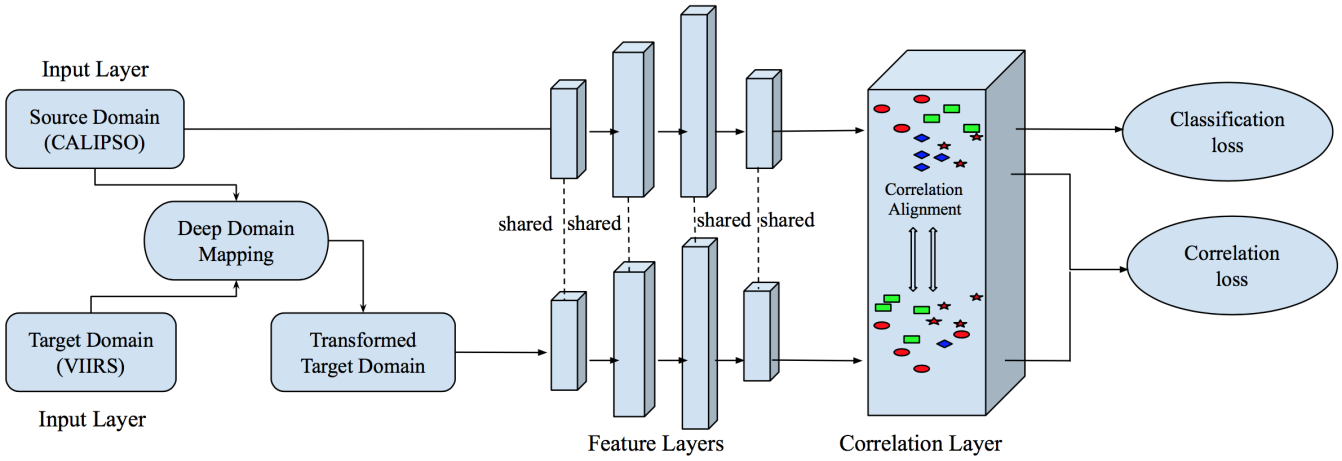

Figure 1: Network Architecture of Deep Multi-Sensor Domain Adaptation with Domain Mapping and Correlation Alignment. Deep Domain Mapping is used to map the target domain into the feature space of source domain. The trained model uses several multilayer perceptron (MLP) layers to learn the shared representative features between the source and target domain. A correlation layer is added to the end of network. In correlation layer, different colors represent different cloud types (labels) that the model aims to classify.

a correlation alignment based method in the homogeneous domain adaptation in computer vision. Its architecture is based on CNN with a classification layer, and a correlation layer is used to minimize the difference in the second-order statistics between the source and target domains. [19] introduced an adversarial learning based domain adaptation method that combines adversarial learning with discriminative feature learning. It specifically learns a discriminative mapping of target images to the source feature space by simultaneously fooling a domain discriminator in distinguishing the encoded target images from source images. The state of art approaches are mostly applicable to solve the homogeneous domain adaptation in image classification, in which the source and target domains are both two dimensional data and share similar feature space. To our knowledge, few of the deep domain adaptation approaches have been used in the remote sensing application or in the heterogeneous domains [22], especially with the heterogeneous nature of datasets collected by active and passive sensors.

3 DEEP MULTIPLE-SENSOR DOMAIN ADAPTATION (DMSDA)

The remote satellite sensing data raises more challenges as the data captured by passive sensor and active Lidar are high dimensional, globally covered and heterogeneous in nature. In this paper, we propose a Deep Multi-Sensor Domain Adaptation approach (DMSDA) and apply it to classify the heterogeneous remote satellite cloud and aerosol types. Our approach introduces a heterogeneous domain matching to map the target domain into the feature space of source domain, and uses shared multilayer perceptron (MLP) layers to train the shared representative features between the source and target domain. At last, it adds a correlation layer to the end of the shared layers, inspired by the idea of correlation alignment introduced in [17]. By incorporating the correlation loss and classification loss in training the domain adaptation network, we find the network can maximize the classification accuracy on the target domain by minimizing the difference in the second-order statistics between the source and target domains. Figure 1 demonstrates our end to end Deep Multi-Sensor Domain Adaptation with domain mapping and correlation alignment.

3.1 Deep Domain Mapping (DDM)

In this section, we explore the heterogeneity of our source (active) and target (passive) remote sensing data, and introduce our Deep Domain Mapping approach to transform the target domain into the feature space of source domain.

3.1.1 ***Heterogeneous Source and Target Domain.*** In heterogeneous domain adaptation, the feature spaces between the source and target domains are nonequivalent and the dimensions may also generally differs [22]. In our satellite remote sensing application, the source (active) domain data, CALIPSO, contains sensing data of 25 attributes collected by the active spaceborne Lidar sensor, shown in Table 1; and the target (passive) domain data, VIIRS, contains another group of sensing data of 20 attributes collected by passive spectroradiometer sensor, shown in 2. From the attribute names and descriptions in the Table 1 and Table 2, we can see the two remote sensing datasets have completely different feature spaces due to the nature of the data they collect. Figure 2 and Figure 3 show the pairwise plot for selected attributes from the source and target domains. The pair plots show CALIPSO and VIIRS have heterogeneous data ranges for each band across the domains. It also reveals the CALIPSO data has better separations for the cloud types as the data are more evenly distributed compared to VIIRS in which the majority data are mixed together in the distribution.

3.1.2 ***Deep Mapping Method.*** To adapt to the completely different feature spaces and heterogeneity of the source and target domain, we introduce a Deep Learning based approach to learn a

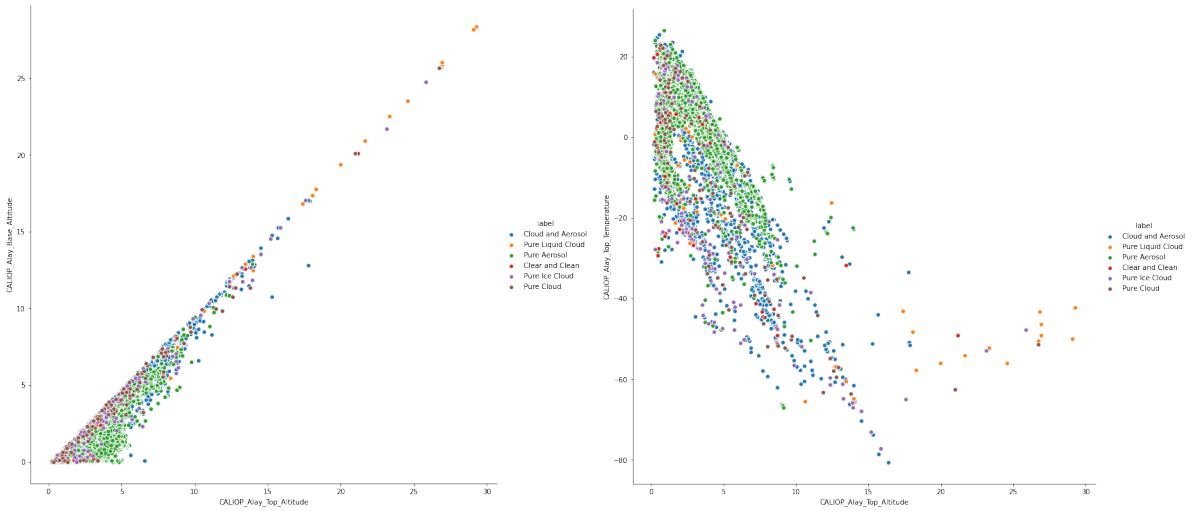

Figure 2: Pairwise relationship plot between CALIOP_Alay_Top_Altitude and CALIOP_Alay_Base_Altitude (Left); CALIOP_Alay_Top_Altitude and CALIOP_Alay_Top_Temperature (Right) in CALIPSO (active) dataset. Different color shows different cloud type (label).

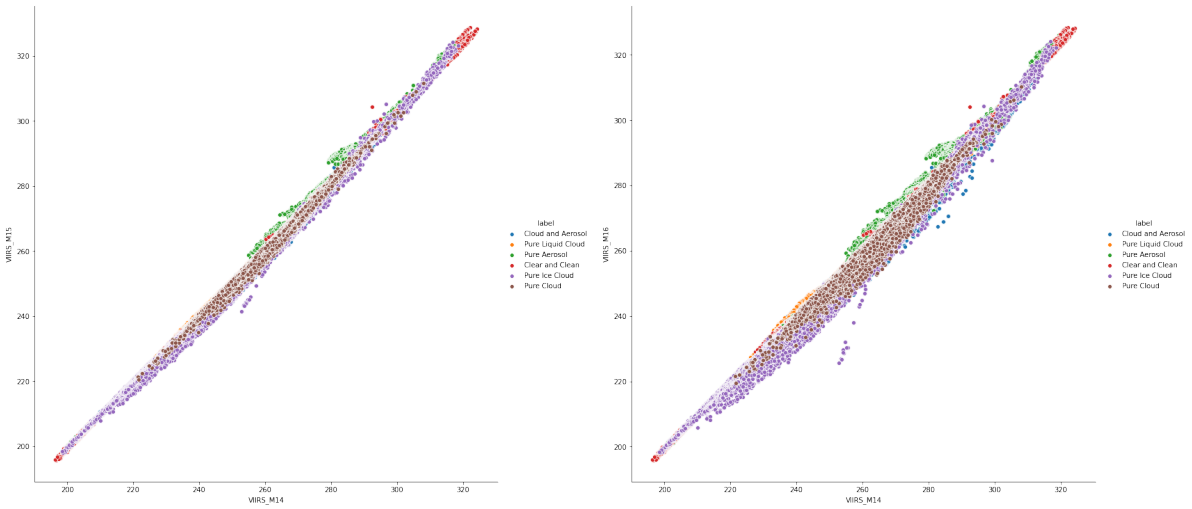

Figure 3: Pairwise relationship plot between VIIRS_M14 and VIIRS_M15 (Left); VIIRS_M14 and VIIRS_M16 (Right) in VIIRS (passive) dataset. Different color shows different cloud type (label).

transformer to map the target feature space into the source feature space. It not only equalizes the number of features in source and target domains, but also aligns the feature distribution by mapping the target domain to source domain.

In our remote sensing dataset, the target domain (VIIRS) has wider spatial coverage but with no label information. The Source domain (CALIPSO) has better representation for cloud types and is fully labeled, so mapping the target domain to source domain can preserve the discriminating power of the source domain and can also transfer it into the down-streaming learner.

We design a deep neural network to perform the Deep Domain Mapping (DDM) between the source and target domain. The input of the Deep Domain Mapping (DDM) network is the target domain data and the output of the network is the transformed target domain data in the source domain feature space. Because the source domain data and target domain data are collocated remote sensing data with the same longitude and latitude coordinates, Mean Square Error (MSE) loss function is used to measure the error of the DDM network. Specifically, given source domain training examples $D_s = \{x_i\}, x \in Rs^{d_s}, i = 1, ..., n_s$ and unlabeled target data set $D_t = \{u_i\}, u \in Rt^{d_t}, i = 1, ..., n_t$, with $d_s \neq d_t$ and $Rs \neq Rt$. Because the source domain and target domain are collocated data so we have $n_s = n_t$. The Deep Domain Mapping network (DDM) is learnt to

Table 1: Attributes/features of CALIPSO satellite sensor.

	Name	Description
1	CALIOP_N_Clay_1km	CALIOP Number of Cloud Layers 1km
2	CALIOP_N_Clay_5km	CALIOP Number of Cloud Layers 5km
3	CALIOP_Liq_Fraction_1km	CALIOP Cloud Layer Liquid Phase Fraction 1km
4	CALIOP_Liq_Fraction_5km	CALIOP Cloud Layer Liquid Phase Fraction 5km
5	CALIOP_Ice_Fraction_1km	CALIOP Cloud Layer Ice Phase Fraction 1km
6	CALIOP_Ice_Fraction_5km	CALIOP Cloud Layer Ice Phase Fraction 5km
7	CALIOP_Clay_Top_Altitude	CALIOP Cloud Layer Top Altitude
8	CALIOP_Clay_Base_Altitude	CALIOP Cloud Layer Base Altitude
9	CALIOP_Clay_Top_Temperature	CALIOP Cloud Layer Top Temperature
10	CALIOP_Clay_Base_Temperature	CALIOP Cloud Layer Base Temperature
11	CALIOP_Clay_Optical_Depth_532	CALIOP Cloud Layer 532nm Optical Depth
12	CALIOP_Clay_Opacity_Flag	CALIOP Cloud Layer Opacity Flag
13	CALIOP_Clay_Integrated_Attenuated_Backscatter_532	CALIOP Cloud Layer Integrated Attenuated Backscatter 532nm
14	CALIOP_Clay_Integrated_Attenuated_Backscatter_1064	CALIOP Cloud Layer Integrated Attenuated Backscatter 1064nm
15	CALIOP_Clay_Final_Lidar_Ratio_532	CALIOP Cloud Layer Lidar Ratio 532nm
16	CALIOP_Clay_Color_Ratio	CALIOP Cloud Layer Color Ratio
17	CALIOP_Alay_Top_Altitude	CALIOP Aerosol Layer Top Altitude
18	CALIOP_Alay_Base_Altitude	CALIOP Aerosol Layer Base Altitude
19	CALIOP_Alay_Top_Temperature	CALIOP Aerosol Layer Top Temperature
20	CALIOP_Alay_Base_Temperature	CALIOP Aerosol Layer Base Temperature
21	CALIOP_Alay_Integrated_Attenuated_Backscatter_532	CALIOP Aerosol Layer Integrated Attenuated Backscatter 532nm
22	CALIOP_Alay_Integrated_Attenuated_Backscatter_1064	CALIOP Aerosol Layer Integrated Attenuated Backscatter 1064nm
23	CALIOP_Alay_Color_Ratio	CALIOP Aerosol Layer Color Ratio
24	CALIOP_Alay_Optical_Depth_532	CALIOP Aerosol Layer 532nm Optical Depth
25	CALIOP_Alay_Aerosol_Type_Mode	CALIOP Aerosol Layer Type

Table 2: Attributes/features of VIIRS satellite sensor.

	Name	Description
1	VIIRS_SZA	viirs solar zenith angle in degree
2	VIIRS_SAA	viirs solar azimuthal angle in degree
3	VIIRS_VZA	viirs viewing zenith angle in degree
4	VIIRS_VAA	viirs viewing azimuthal angle in degree
5	VIIRS_M1	Band wavelength range 0.402-0.422μm
6	VIIRS_M2	Band wavelength range 0.436-0.454μm
7	VIIRS_M3	Band wavelength range 0.478-0.488μm
8	VIIRS_M4	Band wavelength range 0.545-0.565μm
9	VIIRS_M5_B	Band wavelength range 0.662-0.682μm
10	VIIRS_M6	Band wavelength range 0.739-0.754μm
11	VIIRS_M7_G	Band wavelength range 0.846-0.885μm
12	VIIRS_M8	Band wavelength range 1.23-1.25μm
13	VIIRS_M9	Band wavelength range 1.371-1.386μm
14	VIIRS_M10_R	Band wavelength range 1.58-1.64μm
15	VIIRS_M11	Band wavelength range 2.23-2.28μm
16	VIIRS_M12	Band wavelength range 3.61-3.79μm
17	VIIRS_M13	Band wavelength range 3.97-4.13μm
18	VIIRS_M14	Band wavelength range 8.4-8.7μm
19	VIIRS_M15	Band wavelength range 10.26-11.26μm
20	VIIRS_M16	Band wavelength range 11.54-12.49μm

Table 3: Attributes/features shared between CALIPSO and VIIRS.

	Name	Description
1	Latitude	Latitude
2	Longitude	Longitude
3	Surface_Temperature	Surface temperature in Kelvin
4	Surface_Emissivity	Land surface emissivity
5	IGBP_SurfaceType	International Geosphere–Biosphere Programme surface classification
6	SnowIceIndex	Snow/Sea Ice data

transform the target domain into source domain feature space by minimizing L_2 loss function:

$$l_{mse} = \frac{1}{n_t} \sum_{(i=1)}^{n_t} (DDM(u_i) - x_i)^2 \quad (1)$$

Figure 4 shows the network architecture of the Deep Domain Mapping. By minimizing the L_2 error we aim to map the features of the target domain into the feature space of the source domain that has better feature representation. Our Multiple domains experiments in Table 4 show DDM can significantly improve the classification accuracy, demonstrate that domain adaptation and correlation alignment work well on the multiple domains data from the same feature space. The proposed heterogeneous Deep Domain

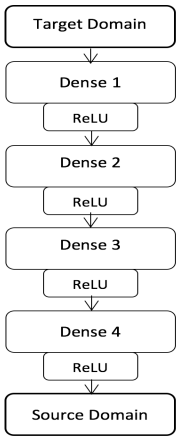

Figure 4: Network Architecture of the Deep Domain Mapping for Heterogeneous Domains

Mapping (DDM) network is also generic and flexible. It can be plugged into other domain adaptation methods and used in areas other than climate data analytics.

3.2 Domain Adaptation with Correlation Alignment

The Domain Adaptation in our DMSDA approach consists of a set of shared MLP feature layers (shown in Figure 1) that is used to extract the domain invariant representation between source and target domain, and a correlation layer that is used to minimize domain shifting by aligning the second order statistics of source and target data distributions.

After transforming the target domain into the feature space of source domain via DDM, the dimension of the transformed target domain is identical to dimension of the source domain and the source domain and target domain become homogeneous. The correlation alignment can be formulated as follows.

Given source domain training examples $D_s = \{x_i\}, x \in R^d$ with labels $L_s = \{y_i\}, i \in \{1, ..., L\}$ and unlabeled transformed target data set $D_t = \{x_i^*\}, x^* \in R^d$, we can compute the covariance matrix of the source domain and target domain, represented as C_s and C_t respectively.

$$C_s = \frac{1}{n_s - 1}(D_s^T D_s - \frac{1}{n_s}(1^T D_s)^T (1^T D_s)) \tag{2}$$

$$C_t = \frac{1}{n_t - 1}(D_t^T D_t - \frac{1}{n_t}(1^T D_t)^T (1^T D_t)) \tag{3}$$

We use the correlation loss proposed in [17] to measure the distance between the second order statistics (covariances) of the source and target data:

$$l_{coral} = \frac{1}{4d^2}||C_s - C_t||_F^2 \tag{4}$$

, where $||.||_F$ denotes the squared matrix Frobenius norm and d is the number of the features.

By combining the correlation loss with the classification loss, the joint loss function is training to learn the latent features that can work well on the target domain:

$$l = l_{class} + \sum_{(i=1)}^{t} \lambda_i l_{coral} \tag{5}$$

Here, t is the number of the correlation layers in the deep network and λ_i is a weight that balances on the adaptation with the classification accuracy on the source domains. The classification loss and the correlation loss play counterparts and reach an equilibrium at the end of training so that the representative capacities of the source domain can be adapted to the target domain, so the final classifier performs well on the target domain with higher accuracy.

3.3 Feature Augmentation

Following our previous work [21], we filter nighttime data records and choose the daytime records with 0 < solar zenith angle (SZA) < 80. Four auxiliary attributes shared in both CALIPSO and VIIRS datasets are surface temperatures, surface emissivity, surface type and snow ice index. The latitude and longitude of the pixel are also provided in both CALIPSO and VIIRS datasets. In total there are 6 auxiliary features (summarized in Table 3) supplemented to both the source and target domains to train the domain adaptation model. The CALIPSO cloud labels are used as reference label information in collocated CALIPSO and VIIRS datasets. A collocation algorithm [9] that fully considers the spatial differences between the two instruments and parallax effects are used to generate our collocated datasets.

4 EXPERIMENTS

We conduct several experiments on real world remote sensing datasets to compare the performance of our proposed model with the state-of-the-art models. Our experiments help us answer the following key questions:

- How does our model (DMSDA) perform against many baseline models including non-domain adaptation and domain adaptation for cloud type prediction?
- What is the impact of deep domain mapping on the model performance?
- What is the impact of correlation alignment on the model performance?

4.1 Datasets and Evaluation Metrics

We conduct experiments on CALIPSO active sensor (source) and VIIRS passive sensor (target) remote satellite sensing datasets[21]. The training dataset is collocated 9-day (Day 101, 102, 106, 112, 114, 118, 122, 126 and 133) CALIPSO and VIIRS datasets containing 700,000 records. We then evaluate each built model by predicting the subsequent 6 days that are Day 138, 142, 144, 147, 154 and 155. Figure 5 shows the number of records in each cloud type (class) for the training and test VIIRS datasets. Analyzing the class distribution in the training dataset, as illustrated in Figure 5, we can see some class imbalance with highest class label data available for 'Pure Liquid' and lowest class label data available for 'Pure Cloud'.

We used Accuracy as the evaluation metric to compare all the models:

$$Accuracy = \frac{\text{Total number of correct predictions}}{\text{Total number of data points}} \tag{6}$$

Table 4: Accuracy on predicting the cloud types on VIIRS (target) dataset.

Models - Single Domain	Source	Target	Training	Validation	Day-138	Day-142	Day-144	Day-147	Day-154	Day-155
Random Forest	VIIRS	VIIRS	0.858	0.824	0.659	0.649	0.658	0.67	0.709	0.655
MLP-CALIPSO	CALIPSO	CALIPSO	1.0	1.0	0.99	0.99	0.99	0.99	0.99	0.99
MLP-VIIRS	VIIRS	VIIRS	0.71	0.7	0.651	0.642	0.647	0.65	0.695	0.636
Models - Multiple Domains	**Source**	**Target**	**Training**	**Validation**	**Day-138**	**Day-142**	**Day-144**	**Day-147**	**Day-154**	**Day-155**
Domain Mapping Only	CALIPSO	VIIRS	0.990	0.670	0.550	0.560	0.530	0.540	0.560	0.530
Correlation Align. Only	CALIPSO	VIIRS	0.990	0.310	0.320	0.316	0.280	0.269	0.282	0.279
DMSDA	CALIPSO	VIIRS	0.990	0.680	0.670	0.660	0.659	0.671	0.704	0.667

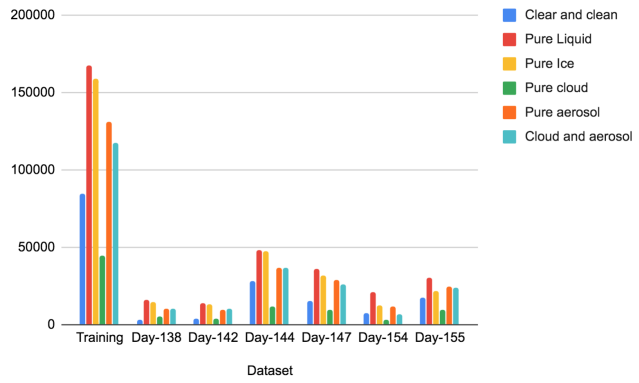

Figure 5: Data distribution (data point count for each cloud type) for training and test VIIRS datasets (Day 138, 142, 144, 147, 154, 155).

4.2 Performance Comparison using data from single domain

For non-domain adaptation model comparison, we conducted experiments on three baseline models which were trained on data from a single domain. These baseline models include 1) RF model: Random Forest trained on VIIRS data, 2) MLP-VIIRS: A deep learning based MLP Model trained on VIIRS data, 3) MLP-CALIPSO: A deep learning based MLP Model trained on CALIPSO data.

In order to make fair comparison to our proposed approach, we apply the same neural network used in the shared layer of our DMSDA network to build the neural network for baseline models (MLP-CALIPSO and MLP-VIIRS), with the same type and number of layers. In our experiments, the MLP (shared) layers are 4 dense layers with 128, 256, 128, 64 neurons respectively, each layer is followed with a ReLU activation function and Dropout (0.5). To train the RF model, we specify 100 as the number of trees and 15 as the maximum depth of the trees in the forest.

As an ML-based baseline result, RF achieves around 85% training, 82% validation and around 70% test accuracy. For the single domain experiments, we can see the MLP-CALIPSO achieves 99% accuracy in predicting the active sensing dataset, which is expected as we can see the data distribution of each cloud type is very discriminative from the CALIPSO pairwise plot shown in Figure 2. In comparison, MLP-VIIRS model has lower accuracy around 65%, as VIIRS is a passive dataset collected by detecting the reflection of natural radiation and their feature discrimination power is weak, which can also be seen in VIIRS pairwise plot in Figure 3. This observation highlights the importance of using multiple sensors data to better understand and classify the unlabeled passive sensing data that has wider spatial coverage. Our proposed deep multi-sensor domain adaptation approach aims to achieve higher accuracy than using single domain data by transferring the discriminating power from the source domain to target domain.

4.3 Performance comparison of using data from multiple domains

For domain adaptation model comparisons, we conducted experiments on two more baseline models that use our heterogeneous domain mapping and correlation alignment respectively, using both source and target datasets. These baseline models include the following: 1) Domain Mapping Only: This model uses the deep domain mapping but no correlation alignment, 2) Correlation Alignment Only: This model uses the Correlation alignment but no Deep Domain Mapping strategy. Comparing these baseline models with our proposed DMSDA model can help understand the importance of each module in our approach.

From the result of multiple sources based models in Table 4, our proposed DMSDA approach outperforms the two domain adaptation baselines significantly. DMSDA improves the accuracy by 23% in average of all the predictions from Day-138 to Day-155 when compared to using the Domain Mapping Only approach. It also has shown almost double accuracy improvement compared to the Correlation Alignment Only approach with domain adaptation that uses the raw source and target features.

4.4 Impact of Domain Mapping

The very low accuracy (around 30%) in predicting the cloud satellite data with Correlation Alignment Only approach exemplifies the inherent complexities in heterogeneous data representation and the challenge of directly applying existing domain adaptation methods in heterogeneous domains. Our proposed Deep Domain Mapping can mitigate the gap between the heterogeneous source and target domains and extract the domain invariant representation by integrating with the domain adaptation technique.

Our DMSDA approach's prediction accuracy is comparable or slightly better than the the widely used Random Forest Model in

climate data analytics. This is reasonable when using the supervised learning approach such as Random Forest in the single target domain assuming the label information is fully available, however, our DMSDA approach is unsupervised domain adaptation that does not require any label information in the target domain, and solely rely on the label information of the source domain and the correlation between the source and target domain to build the model and make the prediction. Moreover, in Domain Adaptation, training on the target domain with target labels is the gold standard in many domain adaptation applications as that's the best the model can achieve. So the domain adaptation performance is upper bounded by the performance on the target domain dataset (i.e. trained on the target data and labels). However, typically in real applications target domain labels are unreliable or unavailable. Our problem setup is slightly different as the target domain labels are obtained from a different satellite (source domain) with co-located latitudes and longitudes.

5 DISCUSSION

Since this work is still in progress, we would like to discuss things we plan to focus on next.

Model Optimization. We will conduct more post analysis to understand what features and components contribute to the improvement of the model performance. We will also improve the domain adaptation network with joint optimization of the DDM *L2* loss with terminal classification loss and correlation alignment loss.

Detailed Evaluation. We will perform more detailed evaluation to understand the capability of our model. First, we will measure accuracy and area under ROC (AUROC) for each of the six labels to know how well the trained model works for each label type. Second, we will study whether the test accuracy of different days is correlated with the similarity of data distribution, namely whether higher data distribution similarity between a test dataset and training dataset will lead to better performance (accuracy) for the test dataset.

Off-track Evaluation. As mentioned in Section 1, passive sensors like VIIRS have better spatial coverage, and our goal is to apply the trained model to predict labels for all VIIRS pixels, a.k.a. off-track pixels, not just those collocated with CALIPSO, a.k.a. in-track pixels. Because we will not have CALIPSO labels for the off-track pixels, one way to evaluate the accuracy our trained model for these pixels is to leverage additional active sensors. For instance, as an active sensor, CloudSat also provides accurate cloud type detection results but its track is different from CALIPSO. We could use CloudSat data as labels to evaluate how good our trained model is for off-track pixels.

Utilizing Weak Labels from VIIRS Dataset. In our current work, cloud information (i.e., the labels) in VIIRS dataset is not used because it is not accurate enough. We plan to study whether the VIIRS cloud information could be used as weak labels to help train our deep learning model because it could provide some information for the off-track pixels. Then our overall learning task will change from unsupervised learning to weakly supervised learning [25] task. We will evaluate whether this approach could help improve the overall prediction accuracy even further.

Model Training with More Dataset. Both VIIRS and CALIPSO have been orbiting the Earth for many years, which means we could expand our model training dataset. We plan to use multiple years of collocated dataset as training data and test on another full year data. In this way, we could get more general model and avoid bias caused by temporal correlation, such as seasonality among the dataset.

Scalable Model Training with Large Dataset. We estimate the overall volume of the above mentioned multi-year dataset will be over 1 TB. To deal with the big dataset, we plan to investigate scalable model training techniques including parallel model training on a GPU cluster and parallel hyperparameter tuning via the integration of big data engines like Spark [1] or Dask [2].

Comparing to Other Deep Domain Adaptation Methods. We plan to explore and compare with other state of art deep domain adaptation methods such as Adversarial Discriminative Domain Adaptation (ADDA) [19]. We would like to integrate our Deep Domain Mapping module with ADDA and evaluate its effectiveness and portability.

Utilizing Neighboring Pixels for Joint Prediction. Our current network architecture trains and tests each pixel record independently. Because remote sensing data are often spatially correlated, we will investigate whether taking into the information of neighboring pixels and use of deep learning models that can capture spatial information (e.g., CNN and / or graph neural networks) could improve the cloud class prediction performance.

Utilizing Spatial Temporal Correlation. Because our data has both spatial and temporal information, one potential improvement on top of our current work is to study how to capture spatial and temporal correlations from data and use them to help prediction. We plan to explore Graph Neural Network models such as Diffusion Convolutional Recurrent Neural Networks [12] for capturing the spatial temporal correlations present in the remote sensing data.

6 CONCLUSIONS

With the advances in remote sensing, we are seeing more and more satellites orbiting the Earth. By utilizing data from multiple satellites jointly, we could achieve better information retrieval for the targeted geophysics variables. Towards this goal, we propose a Deep Multi-Sensor Domain Adaptation method with heterogeneous domain mapping and correlation alignment to employ both active and passive sensing data in cloud type detection. Our experiments show our model can achieve higher accuracy in classifying the challenging passive remote sensing dataset by transferring the representation from the active sensing dataset. For future work, we plan to improve our method further based on the ideas in Discussion section.

ACKNOWLEDGMENTS

This work is supported by grant CyberTraining: DSE: Cross-Training of Researchers in Computing, Applied Mathematics and Atmospheric Sciences using Advanced Cyberinfrastructure Resources (OAC−1730250), grant CAREER: Big Data Climate Causality Analytics (OAC−1942714), and grant CRII (IIS−1948399) from the National Science Foundation.

[1] Apache Spark Project, http://spark.apache.org
[2] Dask: Scalable analytics in Python, https://dask.org

REFERENCES

[1] SA Ackerman, RE Holz, R Frey, EW Eloranta, BC Maddux, and M McGill. 2008. Cloud detection with MODIS. Part II: validation. *Journal of Atmospheric and Oceanic Technology* 25, 7 (2008), 1073–1086.

[2] SA Ackerman, S Platnick, PK Bhartia, B Duncan, T L'Ecuyer, A Heidinger, G Skofronick-Jackson, N Loeb, T Schmit, and N Smith. 2018. Satellites see the world's atmosphere. *Meteorological Monographs* 59 (2018), 4–1.

[3] John Blitzer, Mark Dredze, and Fernando Pereira. 2007. Biographies, bollywood, boom-boxes and blenders: Domain adaptation for sentiment classification. In *Proceedings of the 45th annual meeting of the association of computational linguistics*. 440–447.

[4] Boucher, Randall, Artaxo, Bretherton, Feingold, Forster, Kerminen, Kondo, Liao, Lohmann, Rasch, Satheesh, Sherwood, Stevens, and Zhang. 2013. Clouds and Aerosols. In *Climate Change 2013*. Cambridge University Press, Cambridge, United Kingdom and New York, NY, USA.

[5] Basura Fernando, Amaury Habrard, Marc Sebban, and Tinne Tuytelaars. 2013. Unsupervised visual domain adaptation using subspace alignment. In *Proceedings of the IEEE international conference on computer vision*. 2960–2967.

[6] George Foster, Cyril Goutte, and Roland Kuhn. 2010. Discriminative instance weighting for domain adaptation in statistical machine translation. In *Proceedings of the 2010 conference on empirical methods in natural language processing*. Association for Computational Linguistics, 451–459.

[7] Boqing Gong, Yuan Shi, Fei Sha, and Kristen Grauman. 2012. Geodesic flow kernel for unsupervised domain adaptation. In *2012 IEEE Conference on Computer Vision and Pattern Recognition*. IEEE, 2066–2073.

[8] Kaiming He, Xiangyu Zhang, Shaoqing Ren, and Jian Sun. 2016. Deep residual learning for image recognition. In *Proceedings of the IEEE conference on computer vision and pattern recognition*. 770–778.

[9] RE Holz, SA Ackerman, FW Nagle, R Frey, S Dutcher, RE Kuehn, MA Vaughan, and B Baum. 2008. Global Moderate Resolution Imaging Spectroradiometer (MODIS) cloud detection and height evaluation using CALIOP. *Journal of Geophysical Research: Atmospheres* 113, D8 (2008).

[10] NC Hsu, M-J Jeong, C Bettenhausen, AM Sayer, R Hansell, CS Seftor, J Huang, and S-C Tsay. 2013. Enhanced Deep Blue aerosol retrieval algorithm: The second generation. *Journal of Geophysical Research: Atmospheres* 118, 16 (2013), 9296–9315.

[11] Yann LeCun, Yoshua Bengio, and Geoffrey Hinton. 2015. Deep learning. *nature* 521, 7553 (2015), 436–444.

[12] Yaguang Li, Rose Yu, Cyrus Shahabi, and Yan Liu. 2017. Diffusion convolutional recurrent neural network: Data-driven traffic forecasting. *arXiv preprint arXiv:1707.01926* (2017).

[13] Mingsheng Long, Yue Cao, Jianmin Wang, and Michael I Jordan. 2015. Learning transferable features with deep adaptation networks. *arXiv preprint arXiv:1502.02791* (2015).

[14] José Vanderlei Martins, Didier Tanré, Lorraine Remer, Yoram Kaufman, Shana Mattoo, and Robert Levy. 2002. MODIS cloud screening for remote sensing of aerosols over oceans using spatial variability. *Geophysical Research Letters* 29, 12 (2002), MOD4–1.

[15] Tomas Mikolov, Ilya Sutskever, Kai Chen, Greg S Corrado, and Jeff Dean. 2013. Distributed representations of words and phrases and their compositionality. In *Advances in neural information processing systems*. 3111–3119.

[16] Sanjay Purushotham, Wilka Carvalho, Tanachat Nilanon, and Yan Liu. 2016. Variational recurrent adversarial deep domain adaptation. (2016).

[17] Baochen Sun and Kate Saenko. 2016. Deep coral: Correlation alignment for deep domain adaptation. In *European conference on computer vision*. Springer, 443–450.

[18] Eric Tzeng, Judy Hoffman, Trevor Darrell, and Kate Saenko. 2015. Simultaneous deep transfer across domains and tasks. In *Proceedings of the IEEE International Conference on Computer Vision*. 4068–4076.

[19] Eric Tzeng, Judy Hoffman, Kate Saenko, and Trevor Darrell. 2017. Adversarial discriminative domain adaptation. In *Proceedings of the IEEE Conference on Computer Vision and Pattern Recognition*. 7167–7176.

[20] Eric Tzeng, Judy Hoffman, Ning Zhang, Kate Saenko, and Trevor Darrell. 2014. Deep domain confusion: Maximizing for domain invariance. *arXiv preprint arXiv:1412.3474* (2014).

[21] Chenxi Wang, Steven Platnick, Kerry Meyer, Zhibo Zhang, and Yaping Zhou. 2020. A machine-learning-based cloud detection and thermodynamic-phase classification algorithm using passive spectral observations. *Atmospheric Measurement Techniques* 13, 5 (2020), 2257–2257.

[22] Mei Wang and Weihong Deng. 2018. Deep Visual Domain Adaptation: A Survey. *Neurocomputing* 312 (2018), 135–153.

[23] Liangpei Zhang, Lefei Zhang, and Bo Du. 2016. Deep learning for remote sensing data: A technical tutorial on the state of the art. *IEEE Geoscience and Remote Sensing Magazine* 4, 2 (2016), 22–40.

[24] Wenbin Zhang, Jianwu Wang, Daeho Jin, Lazaros Oreopoulos, and Zhibo Zhang. 2018. A deterministic self-organizing map approach and its application on satellite data based cloud type classification. In *2018 IEEE International Conference on Big Data (Big Data)*. IEEE, 2027–2034.

[25] Zhi-Hua Zhou. 2018. A brief introduction to weakly supervised learning. *National Science Review* 5, 1 (2018), 44–53.